RESEARCH ARTICLE | MARCH 06 2025

Predictive model for non-Newtonian droplet impact on moving solid surfaces

Haicui Wang (王海翠); Long Shen (沈龙); Lunliang Duan (段伦良) ; Xinxin Li (李鑫鑫); Zhimin Ma (马志敏); Pengfei Li (李鹏飞); Kui Wang (汪魁)

Physics of Fluids 37, 033112 (2025)
https://doi.org/10.1063/5.0253692

Physics of Fluids ARTICLE pubs.aip.org/aip/pof

Predictive model for non-Newtonian droplet impact on moving solid surfaces

Cite as: Phys. Fluids **37**, 033112 (2025); doi: 10.1063/5.0253692
Submitted: 18 December 2024 · Accepted: 5 February 2025 ·
Published Online: 6 March 2025

Haicui Wang (王海翠),[1,2,3] Long Shen (沈龙),[1] Lunliang Duan (段伦良),[1,a)] Xinxin Li (李鑫鑫),[1] Zhimin Ma (马志敏),[4] Pengfei Li (李鹏飞),[1] and Kui Wang (汪魁)[1]

AFFILIATIONS

[1]College of River and Ocean Engineering, Chongqing Jiaotong University, Chongqing 400074, China
[2]Faculty of Construction and Environment, The Hong Kong Polytechnic University, Hong Kong 999077, China
[3]National Key Laboratory for Bridge Engineering Safety and Resilience, Chongqing 400067, China
[4]Chongqing Yushendi Industrial Co., Ltd., Chongqing 402283, China

[a)]Author to whom correspondence should be addressed: duanll89@126.com

ABSTRACT

We have developed a refined predictive model for the spreading dynamics of non-Newtonian droplets impacting both stationary and moving surfaces. Using numerical simulations, the key physical mechanisms, including inertial spreading, shear-thinning effects, and capillary stabilization, were identified and integrated into the model. The model extends classical Newtonian frameworks by incorporating the time-dependent and shear-rate-dependent rheological properties of non-Newtonian fluids. The numerical framework employs the volume of fluid method combined with dynamic contact angle modeling to resolve interface dynamics and wetting behavior. Comparisons with experimental data for shear-thinning droplets (e.g., Parafilm-M at We = 24 and We = 94) demonstrated strong agreement within a 3% margin of error, confirming the model's accuracy. Notably, the model successfully captures anisotropic spreading induced by surface motion, a phenomenon neglected in prior studies. Notably, the model accurately captured anisotropic spreading induced by surface motion, a phenomenon neglected in existing frameworks. The results highlight the model's robustness in generalizing across trained and untrained conditions, emphasizing its applicability for industrial processes such as inkjet printing, spray coating, and pharmaceutical droplet deposition. This work establishes a comprehensive framework for understanding and predicting the complex dynamics of non-Newtonian droplet impacts.

I. INTRODUCTION

Droplet impact dynamics are fundamental to numerous industrial and scientific applications, including inkjet printing, spray coating, and pharmaceutical deposition. The behavior of a droplet during impact, encompassing spreading, recoiling, and stabilization, results from the complex interplay of inertial, viscous, and capillary forces. For Newtonian fluids, dimensionless parameters such as the Weber and Ohnesorge numbers provide robust frameworks for predicting transitions between inertial and capillary regimes. The Weber number encapsulates the ratio of inertial to surface tension forces, while the Ohnesorge number quantifies the influence of viscosity on deformation. Foundational studies by Josserand and Thoroddsen[1] and Yarin[2] elucidated these parameters' role in droplet spreading dynamics, particularly on static surfaces. Furthering this understanding, Gorin *et al.*[3] established universal scaling laws for droplet spreading applicable to both Newtonian and non-Newtonian fluids, demonstrating that appropriately rescaled spreading dynamics collapse onto a single master curve. Their findings provide a general framework for characterizing spreading across a wide range of impact conditions.

Substrate properties, including texture, wettability, and motion, significantly influence Newtonian droplet behavior. Bird *et al.*[4] identified asymmetries in spreading patterns induced by surface motion, while Mehdizadeh *et al.*[5] explored enhanced splashing on heated substrates due to rapid evaporation. Meanwhile, Snoeijer and Andreotti[6] developed a theoretical framework for analyzing moving contact lines on textured surfaces. Expanding on this, Abdelsayed *et al.*[7] conducted direct numerical simulations to investigate primary atomization of shear-thinning liquid jets, revealing how non-Newtonian behavior alters breakup regimes and influences droplet morphology. These findings underscore the need to account for surface-specific effects when modeling droplet impact dynamics.

While Newtonian droplet dynamics have been extensively studied, the impact behavior of non-Newtonian fluids, particularly shear-thinning liquids, remains less explored. Shear-thinning fluids, such as polyethylene oxide (PEO) solutions, exhibit viscosity reductions with increasing shear rates, enhancing spreading and modifying recoil dynamics.[8] The addition of viscoelastic properties introduces complexity, allowing energy storage during deformation, which can suppress rebound and improve adhesion. Shah and Driscoll[9] reviewed the role of rheological properties in complex fluid dynamics, emphasizing the need for comprehensive models. Studies by Andrade *et al.*[10] and Guémas *et al.*[11] highlighted the importance of adapting classical models to account for shear-thinning effects, particularly for predicting maximum spreading factors. Complementing these works, Li *et al.*[12] numerically investigated the secondary breakup of shear-thinning droplets, demonstrating how their effective viscosity distribution influences droplet fragmentation and shape evolution under impact conditions. Their findings contribute to refining predictive models for droplet disintegration in industrial applications. Mousavi *et al.*[13] explored droplet detachment from solid surfaces under gravity using the lattice Boltzmann method, shedding light on the forces governing liquid adhesion and detachment dynamics.

Research on non-Newtonian droplet impact has revealed unique behaviors. Boyer *et al.*[14] showed that shear-thickening fluids exhibit reduced spreading compared to Newtonian fluids under similar conditions, while An and Lee[15] observed that surface wettability plays a minor role at high Weber numbers. Numerical studies, including the one by Yang *et al.*,[16] employed the volume of fluid (VOF) method and dynamic contact angle (DCA) modeling to investigate shear-thinning droplets on static and dynamic surfaces, emphasizing the need for advanced predictive frameworks. Further supporting this, Cai *et al.*[17] examined shear-thinning droplets impacting hydrophobic spherical surfaces using VOF modeling and dynamic contact angle simulations, providing insights into film thickness, contact line dynamics, and spreading factors under different impact conditions. Their study offers a valuable perspective on droplet interactions with non-planar surfaces.

Dynamic conditions, such as moving surfaces, present additional challenges, inducing anisotropic spreading and altered contact angles. Chandra and Avedisian[18] explored the role of impact velocity in spreading and splashing dynamics. Building on this, Biroun *et al.*[19] performed experimental studies on non-Newtonian droplets impacting superhydrophobic surfaces, revealing how Xanthan gum concentration affects rebound behavior and significantly reduces contact time. Their findings have practical implications for coatings, inkjet printing, and biomedical applications where droplet adhesion control is crucial. Tilehboni *et al.*[20] also numerically investigated droplet deformation and breakup under gravity using the lattice Boltzmann method, providing insights into detachment behavior and interfacial forces affecting droplet stability.

Using the volume of fluid (VOF) method combined with a dynamic contact angle (DCA) model, this study develops a predictive framework to investigate the impact dynamics of shear-thinning PEO droplets on both stationary and moving surfaces. The numerical model considers a wide range of droplet sizes (0.5–1.5 mm), impact velocities (0.5–1.5 m/s), and surface velocities (0.5–1.5 m/s), along with relevant Weber (We = 12.5–112.5) and Ohnesorge (Oh = 0.115–0.200) numbers to systematically analyze the interplay of inertial, viscous, and capillary forces during spreading.

The proposed model extends classical Newtonian frameworks by incorporating shear-thinning viscosity effects, anisotropic spreading, and time-dependent energy redistribution under dynamic impact conditions. The numerical approach is implemented in ANSYS Fluent, with Kistler's dynamic contact angle model used to capture interface evolution. To improve accuracy in modeling droplet retraction, the dynamic receding contact angle model[21] is also incorporated. This study aims to quantify the influence of shear-thinning behavior on spreading dynamics, assess the role of surface motion in modifying impact outcomes, and provide a comprehensive framework for optimizing droplet behavior in industrial applications such as inkjet printing, spray coating, and pharmaceutical deposition.

II. NUMERICAL METHODOLOGY

A. Governing equations

The numerical simulation of drop spreading and impact dynamics for non-Newtonian fluids exhibiting shear-thinning behavior involves two distinct phases. To handle the fluid interface accurately, the volume of fluid (VOF) method is employed. This method, based on an Eulerian framework, efficiently captures interface deformations.

The governing equations for incompressible flows are modified to account for the non-Newtonian behavior,

$$\nabla \cdot \vec{U} = 0,$$

$$\frac{\partial \alpha}{\partial t} + \nabla \cdot (\vec{U}\alpha) = 0,$$

$$\frac{\partial}{\partial t}(\rho \vec{U}) + \nabla \cdot (\rho \vec{U} \otimes \vec{U}) = -\nabla p + \nabla \cdot \left[\mu_{eff}\left(\nabla \vec{U} + (\nabla \vec{U})^T - \frac{2}{3}(\nabla \cdot \vec{U})I\right)\right] + \rho \vec{a} + F_s.$$

B. Non-Newtonian power-law shear-thinning viscosity

For shear-thinning fluids, the viscosity μ_{eff} follows the power-law model,

$$\mu_{eff} = K \dot{\gamma}^{n-1},$$

where K is the consistency index, n is the flow behavior index (for shear-thinning $n < 1$), and $\dot{\gamma}$ is the shear rate magnitude, defined as

$$\dot{\gamma} = \sqrt{2\, D : D},$$

where $D = 1/2\left(\nabla \vec{U} + (\nabla \vec{U})^T\right)$ represents the strain rate tensor.

The effective viscosity μ_{eff} is applied locally in the momentum equation to capture the shear-dependent viscosity variations.

The interface between the phases is modeled using the modified VOF transport equation, which includes an additional compression term to ensure sharpness,

$$\frac{\partial \alpha}{\partial t} + \nabla \cdot (\vec{U}\alpha) + \nabla \cdot \left(\left(\vec{U} - \vec{U}_l\right)\alpha(1-\alpha)\right) = 0.$$

The fluid properties (density ρ and viscosity μ_{eff}) are computed based on the volume fraction α,

$$\mu_{eff} = \alpha\, \mu_{eff,1} + (1-\alpha)\mu_{eff,2},$$

$$\rho = \alpha\, \rho_1 + (1-\alpha)\rho_2.$$

The capillary force is modeled using the continuum surface force (CSF) approach,[22] where the surface force F_s is expressed as

$$F_s = \gamma\,\kappa\,\nabla\alpha,\ \kappa = -\nabla\cdot\left(\frac{\nabla\alpha}{|\nabla\alpha|}\right).$$

Here, κ represents the curvature of the interface, and γ is the surface tension coefficient.

To accurately predict the interface shape near the three-phase contact line, the unit normal of the interface $\hat{n}$ is adjusted using the dynamic contact angle θ_d,

$$\hat{n} = \frac{\nabla\gamma}{|\nabla\gamma|} = \hat{n}_w\cos\theta_d + \hat{n}_t\sin\theta_d.$$

Here, $\hat{n}$ and $\hat{n}_w$ are the unit vectors of the solid surface in the tangential and normal directions. The contact angle varies due to contact angle hysteresis $\theta_A - \theta_R$ dynamic contact angle depends on several factors, including the contact line velocity and droplet properties. Various models predict the dynamic contact angle during spreading or retraction, such as Shikmurzaev's model,[23] Cox's model,[24] and Kistler's model.[25] In this study, Kistler's model is implemented as a User-Defined Function (UDF) in ANSYS Fluent,

$$\theta_d = f_H\left[Ca + f_H^{\{-1\}(\theta)}\right],$$

$$f_H = \cos^{-1}\left(1 - 2\tanh\left(5.16\left(\frac{\tau}{1+1.31\,\tau^{0.99}}\right)^{0.706}\right)\right),$$

where θ_d represents the dynamic contact angle as a function of the contact line velocity (u_d), expressed as the capillary number $Ca = \mu\frac{u_d}{\gamma}$, and θ_d is shown as a function of Ca using Hoffman's function (f_H). The bulk contact line motion is truly multi-scale, and more accurate predictions might require a molecular perspective. As the Kistler's model does not account for receding contact angles, one possible approach is to use the dynamic receding contact angle model introduced by Nichita *et al.*,[21] where the receding contact angle can be calculated using the equation $\theta_D = \left(\theta_R^3 - 72Ca\right)^{\frac{1}{3}}$.

C. Numerical implementation

The governing equations are discretized and solved using the ANSYS Fluent library. Adaptive time-stepping based on the CFL condition is employed to ensure numerical stability.

III. RESULTS AND DISCUSSION

The objective of this study is to develop a predictive model for the spreading dynamics of non-Newtonian droplets. To achieve this, we analyze numerical simulation results to identify key physical mechanisms, including elongation, edge thinning, and phase transitions, which guide the model development. Simulations were conducted under varying velocity and surface motion conditions using the Power Law framework to capture shear-thinning effects.

The simulations were performed using ANSYS Fluent, modeling the droplet with the Power Law framework to capture shear-thinning effects. Parameters were chosen to represent typical polymer solutions, with a flow behavior index ($n = 0.5$), indicating strong shear-thinning behavior, and a consistency index ($K = 1\ \text{Pa}\cdot\text{s}$). The droplet's density ($\rho = 1000\,\frac{\text{kg}}{\text{m}^3}$) and surface tension ($\sigma = 0.05\,\frac{\text{N}}{\text{m}}$) ensured realistic physical properties. Initial droplet velocities (v_n) ranged from 0.5 to 1.5 m/s, and surface velocities (v_s) were varied between 0.5 and 1.5 m/s, yielding Weber numbers (We) from 12.5 to 112.5 and Ohnesorge numbers (Oh) from 0.115 to 0.200. Key metrics, such as the maximum elongation (L_{max}) and the time evolution of the spreading factor, were analyzed to characterize the droplet's dynamics. The observed trends provide the basis for the development of a refined model that incorporates the interplay of inertial, viscous, and capillary forces alongside the unique rheological properties of non-Newtonian fluids.

A. Validation of simulations against experimental results

The simulation results were validated against experimental data for Parafilm-M droplets impacting a surface at two Weber numbers, We = 24 and We = 94. The droplets are characterized by high zero-shear viscosity and significant shear-thinning behavior, represented by X0.35, as detailed in the experimental study by An and Lee.[15]

For We = 24 with an impact velocity of $V_n = 0.8$ m/s, the experimental data show a maximum spreading factor of $\beta \approx 1.98$ at $t \approx 3.3$ ms. The simulated results closely replicate this trend, capturing both the rapid initial rise and subsequent slight decline in β. The agreement remains within a 3% margin of error, confirming the model's accuracy.

At We = 94 and a higher impact velocity of $V_n = 1.6$ m/s, the maximum spreading factor increases to $\beta \approx 2.65$, occurring at a similar time of $t \approx 3.3$ ms. The simulation demonstrates a steeper initial increase due to the higher inertia, followed by a gradual decrease. The comparison between experimental and simulated data again shows excellent agreement, with deviations consistently below 3%.

These results confirm that increasing the Weber number enhances the spreading factor, as inertial forces become more dominant than viscous and capillary effects. Moreover, the strong correlation between simulations and experiments validates not only the numerical model but also the applied mesh refinement strategy and computational stability (Fig. 1).

The following, first present the results of the numerical simulations, detailing the droplet's behavior on static and moving surfaces. These findings then inform the formulation, optimization, and validation of a predictive spreading model capable of capturing non-Newtonian dynamics across diverse conditions.

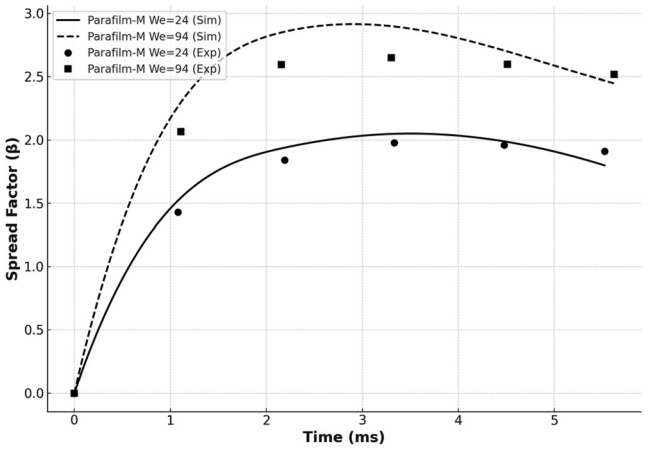

FIG. 1. Comparison between simulated and experimental spreading factors (β) of An and Lee[15] for Parafilm-M droplets at We = 24 and We = 94. Experimental data are shown as symbols, and simulation results as lines.

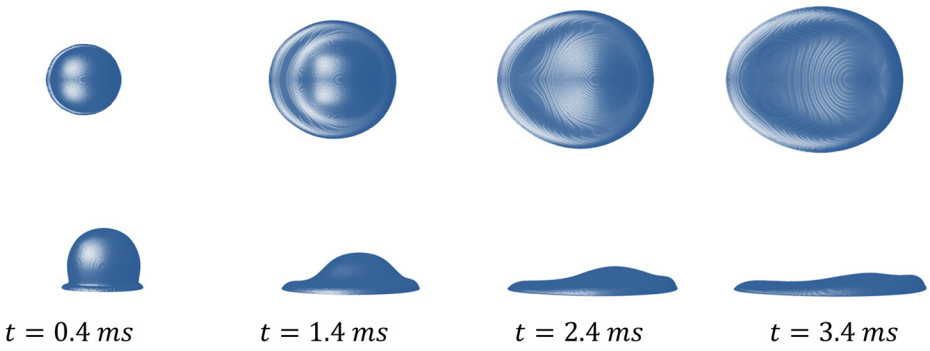

FIG. 2. Time evolution of droplet spreading for $v_n = 1.0$ m/s and $v_s = 1.0$ m/s at four distinct time intervals: t = 0.4 ms, t = 1.4 ms, t = 2.4 ms, and t = 3.4 ms. The overhead views (top row) and side views (bottom row) illustrate the progression of the lamella from circular spreading in the initial phase to an elliptical deformation in the late phase.

B. Time evolution of lamella dynamics

The dynamics of a non-Newtonian droplet impacting a moving surface were analyzed to investigate the evolution of the lamella shape over time. Figure 2 illustrates four distinct phases of spreading: initial, intermediate, late, and final. In the initial phase (t = 0.4 ms), the droplet undergoes rapid expansion upon impact, with the lamella spreading symmetrically in a nearly circular shape, as observed in the overhead view. The dominance of inertial forces during this phase results in significant vertical height retention, as shown in the side view, with minimal contributions from viscous forces or surface motion.

As the droplet progresses to the intermediate phase (t = 1.4 ms), the lamella begins to elongate along the axis of surface motion, reflecting the redistribution of kinetic energy from vertical deformation to lateral spreading. Shear-thinning effects become apparent, moderating the spreading rate and resulting in edge thinning. The influence of viscous and surface forces increases, signaling a transition from the inertia-dominated regime.

In the late phase (t = 2.4 ms), the lamella adopts a pronounced elliptical shape, with elongation along the surface motion axis dominating the dynamics. The interplay between surface motion and non-Newtonian viscosity becomes evident, as capillary forces gradually stabilize the spreading process. The side view reveals continued edge thinning, characteristic of the shear-thinning fluid, which reduces resistance to flow at higher deformation rates. Finally, the lamella approaches its maximum lateral extent and stabilizes under the influence of surface tension forces at 3.4 ms after the impact. The overhead view shows that elongation along the surface motion axis becomes negligible, while the side view confirms the near-complete dissipation of vertical energy. The resulting lamella is highly elongated and thin, reflecting the unique interplay of shear-thinning behavior, surface velocity, and capillary forces.

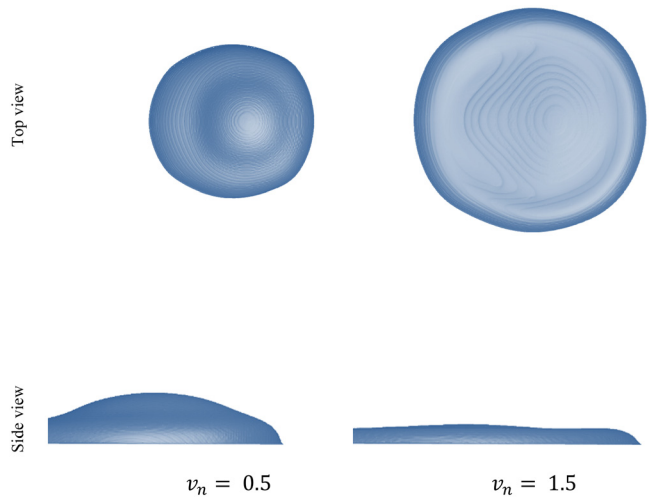

FIG. 3. Lamella shapes at t = 1.5 ms for different droplet velocities (v_n) at a constant surface velocity ($v_s = 0.5$ m/s). Left: $v_n = 0.5$ m/s; right: $v_n = 1.5$ m/s. Overhead views (top row) illustrate spreading symmetry and elongation, while side views (bottom row) reveal lamella height and edge thinning.

C. Effect of droplet velocity on lamella morphology

At a surface velocity of $v_s = 0.5$ m/s, the lamella dynamics are significantly influenced by variations in droplet velocity (v_n). Figure 3 compares the lamella shapes for $v_n = 1.5$ m/s and $v_n = 0.5$ m/s at t = 1.5 ms, illustrating the combined effects of inertia, viscosity, and surface forces. At higher droplet velocity ($v_n = 1.5$ m/s), the lamella exhibits pronounced elongation along the surface motion axis, as seen in the overhead view, highlighting the dominance of inertial forces. The edges are visibly thinner, reflecting the enhanced influence of shear-thinning viscosity at higher deformation rates. Simultaneously, the side view reveals a significant reduction in lamella height, indicating efficient redistribution of kinetic energy into lateral spreading.

In contrast, for lower droplet velocity ($v_n = 0.5$ m/s), the lamella retains a more circular shape with thicker edges, as seen in the overhead view. The reduced shear rates at lower velocities result in diminished thinning effects. The side view further shows that vertical deformation persists longer, as indicated by the greater lamella height, reflecting slower energy redistribution into lateral spreading.

These observations demonstrate the dual impact of droplet velocity on lamella morphology: higher velocities amplify inertial effects, leading to greater elongation and pronounced edge thinning, while lower velocities result in more symmetric lamella shapes with reduced thinning. This sensitivity of lamella dynamics to droplet inertia provides critical insights for applications requiring precise control of spreading behavior, such as high-speed coating or printing processes.

The impact of normal velocity (v_n) at high surface velocity (v_s) on lamella dynamics is presented in Fig. 4. At higher normal velocity ($v_n = 1.5$), the lamella undergoes significant elongation along the direction of surface motion, as seen in the overhead view. This elongation is far more pronounced than at low surface velocities, where inertial spreading dominates symmetrically. The side view reveals considerable edge thinning and a marked reduction in lamella height,

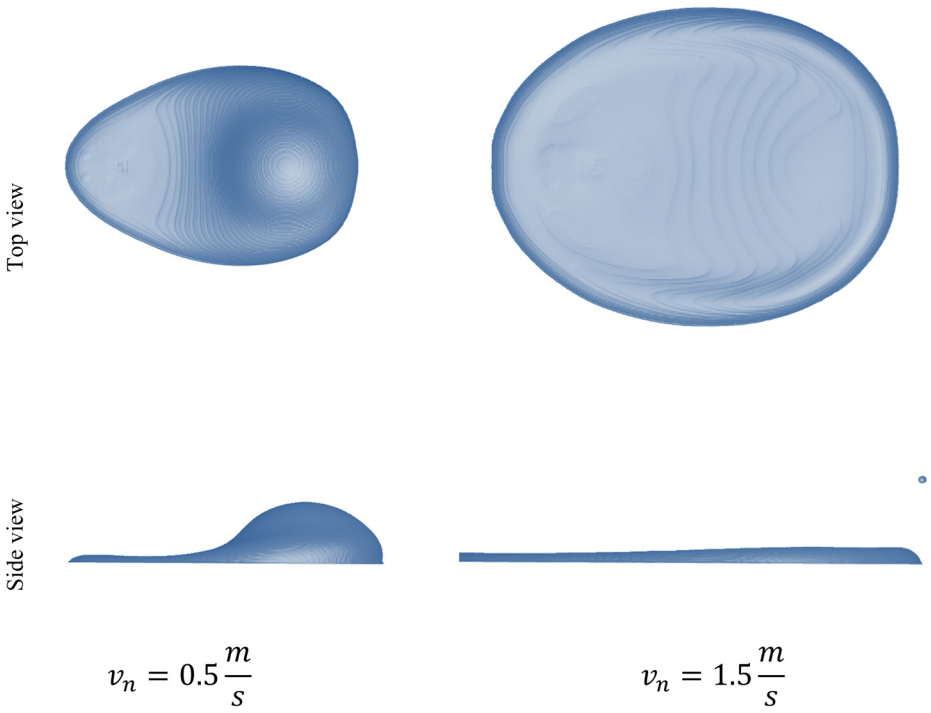

FIG. 4. Lamella shapes at t = 1.5 ms for different droplet velocities (v_n) at a constant surface velocity (v_s = 1.5 m/s). Left: v_n = 0.5 m/s; right: v_n = 1.5 m/s. Overhead views (top row) illustrate the lamella elongation along the surface velocity direction, while side views (bottom row) highlight differences in lamella height and edge thinning.

highlighting the efficient lateral redistribution of kinetic energy enhanced by shear-thinning effects at higher deformation rates.

In contrast, at lower normal velocity ($v_n = 0.5\,m/s$), the lamella remains more compact and asymmetric. While elongation still occurs due to surface motion, it is less pronounced compared to the high normal velocity case. The side view shows greater vertical retention and thicker edges, reflecting reduced inertial input and lower shear rates, consistent with observations at lower surface velocities.

Compared to low surface velocity conditions, the high surface velocity ($v_s = 1.5\,m/s$) significantly enhances anisotropic spreading and edge thinning, particularly at higher normal velocities. These results emphasize the combined influence of surface motion and

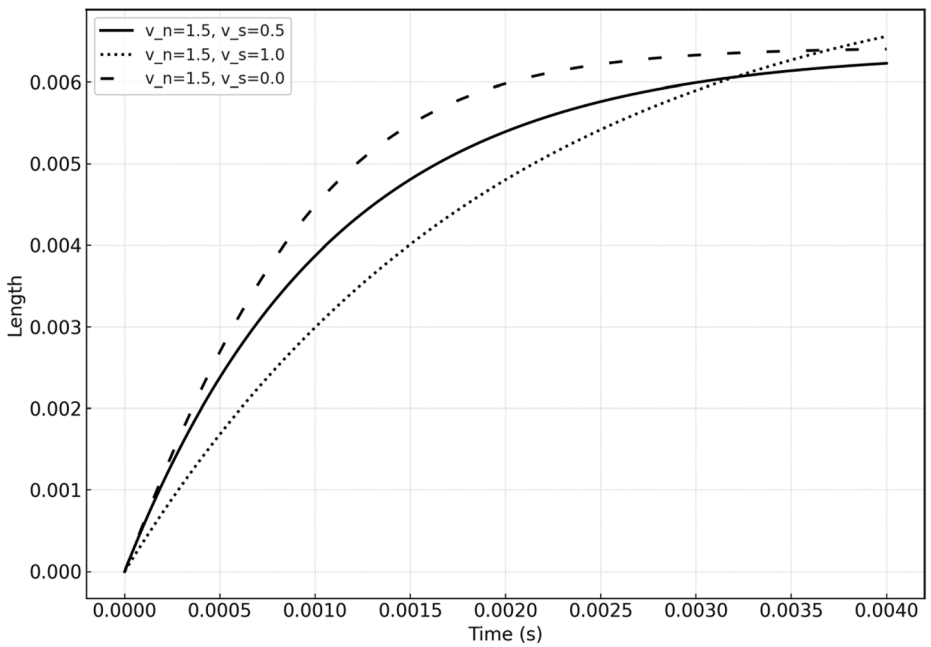

FIG. 5. Time evolution of the lamella length for different surface velocities (v_s = 0.0, 0.5, 1.0 m/s) at a constant normal velocity (v_n = 1.5 m/s). The solid line represents v_s = 0.5 m/s, the dashed line shows v_s = 1.0 m/s, and the dotted line corresponds to v_s = 0.0 m/s.

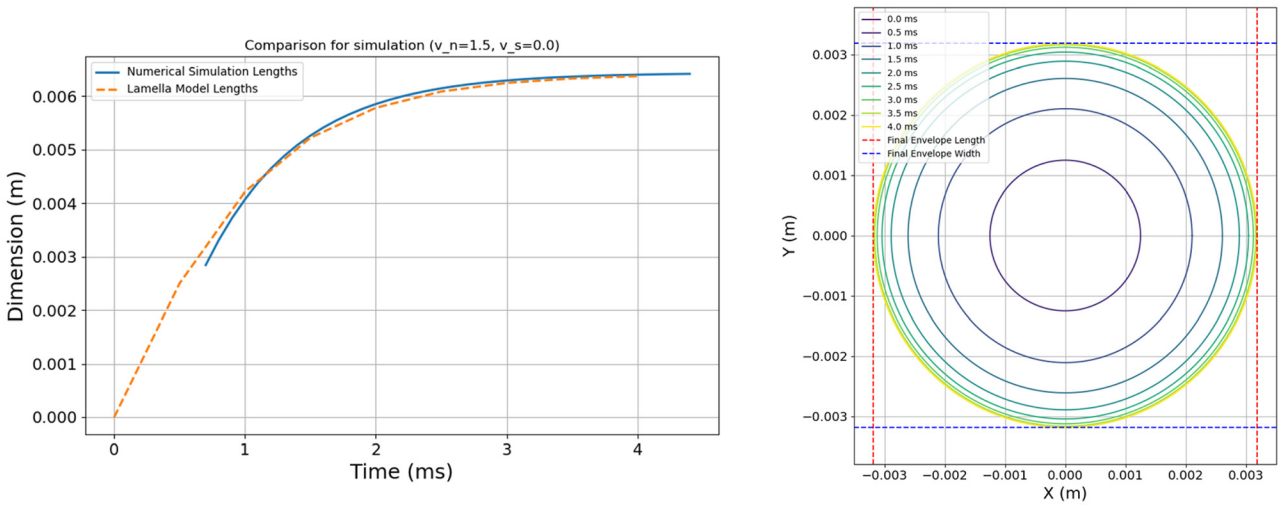

FIG. 6. Validation of the developed model for $v_n = 1.5$ m/s on a static surface. The left panel shows a comparison between the model predictions and numerical simulation results for the droplet's spreading factor. The right panel illustrates the lamella's shape at different time intervals, highlighting its evolution and the final stabilized shape.

impact energy in driving lamella deformation and highlight the sensitivity of spreading dynamics to both normal and surface velocities.

The time evolution of lamella length at a constant impact velocity ($v_n = 1.5$ m/s) for varying surface velocities ($v_s = 0.0, 0.5, 1.0$ m/s) is presented in Fig. 5. This figure demonstrates the effect of surface motion on the elongation dynamics and stabilization of the lamella.

At $v_s = 0.0$ m/s (static surface), the lamella length increases symmetrically and stabilizes earlier, with the growth driven primarily by inertial spreading balanced by capillary forces. As surface velocity increases to $v_s = 0.5$ m/s, the lamella exhibits greater elongation, particularly during the intermediate phase. The surface motion redistributes kinetic energy along the motion axis, enhancing anisotropic spreading. The differences in growth rates become most prominent after $t \sim 0.001$ s, when surface motion begins to dominate the spreading dynamics. These results emphasize the need to account for surface velocity effects when developing predictive models for non-Newtonian droplet spreading.

While models for Newtonian droplet dynamics are well-established, they fail to describe the unique behavior of shear-thinning fluids, where viscosity decreases with increasing shear rates. For Newtonian droplets, spreading is typically captured by scaling laws based on dimensionless Weber and Ohnesorge numbers, successfully predicting the transition from inertia-driven spreading to capillary and viscous stabilization. These models, however, cannot account for enhanced edge thinning and anisotropic spreading observed in shear-thinning droplets, particularly under surface motion.

D. Spreading model

To address this gap, we propose a refined spreading factor model tailored for non-Newtonian fluids. The model incorporates time-dependent shear-thinning viscosity effects and surface motion, building upon the Newtonian framework while capturing the complex rheological behavior observed in simulations. The spreading factor, $\frac{D(t)}{D_{max}}$, is

$$\frac{D(t)}{D_{max}} = \left(\frac{D_{max}}{D_0}\right)\left[1 - \exp\left(-\alpha \cdot t^{\gamma} \cdot We^{\delta} \cdot Oh^{-\beta}\right)\right].$$

- $D(t)$: Time-dependent lamella diameter.
- D_{max}: Maximum lamella diameter.
- D_0: Initial droplet diameter.
- $We = \frac{\rho v_n^2 D_0}{\sigma}$: Weber number, representing the ratio of inertial to surface tension forces.
- $Oh = \frac{\mu_{\text{eff}}}{\sqrt{\rho\,\sigma D_0}}$: Ohnesorge number, quantifying the relative importance of viscous forces.
- $\alpha, \beta, \gamma, \delta$: Empirical parameters capturing time-dependence, inertial effects, and the influence of viscous dissipation.

The Weber and Ohnesorge numbers remain fundamental in describing droplet impact dynamics by characterizing the interplay of inertial, viscous, and capillary forces. However, for non-Newtonian fluids, the Ohnesorge number must be modified to account for shear-thinning viscosity, where the fluid's resistance decreases at higher shear rates. Specifically, the effective viscosity (μ_{eff}) is not constant but varies with the shear rate, necessitating adjustments to the scaling parameter β in the proposed model.

Additionally, the time-dependent parameter γ reflects the delayed redistribution of kinetic energy caused by reduced viscous resistance at high deformation rates. This modification is critical for capturing the spreading dynamics unique to shear-thinning droplets, where edge thinning and anisotropic elongation are more pronounced compared to Newtonian fluids.

By integrating these rheological effects, the refined model bridges the limitations of Newtonian frameworks, providing a robust and accurate prediction of lamella dynamics across diverse impact and surface conditions.

E. Validation and analysis of the refined spreading model

1. Static surface validation

The developed model was validated by comparing its predictions to numerical simulation results for a non-Newtonian droplet

impacting a static surface at $v_n = 1.5$ m/s, as shown in Fig. 6. The left panel presents the time evolution of the lamella length, demonstrating excellent agreement between the model and simulation results across all phases. In the initial phase, inertial forces drive rapid lamella expansion, which is accurately captured by the model. As the system transitions to the intermediate and late phases, shear-thinning effects modulate the spreading dynamics, delaying stabilization compared to Newtonian fluids. The model successfully incorporates this effect through the interplay of the empirical parameters $(\alpha, \beta, \gamma, \delta)$. The right panel illustrates the evolution of the lamella shape at several time intervals. The progression from a circular, inertia-dominated spreading phase to a final stabilized symmetric shape highlights the contributions of viscous and capillary forces. The close agreement between the model and simulation results underscores the model's capability to capture the key transitions in lamella morphology.

These results validate the robustness of the refined model in accurately predicting lamella dynamics for shear-thinning droplets on stationary surfaces. By integrating the effects of inertial spreading, shear-thinning viscosity, and surface tension, the model offers a reliable framework for analyzing non-Newtonian droplet behavior.

2. Dynamic surface validation

The performance of the refined model is further examined for a moving surface with a velocity of $v_s = 1.0$ m/s. Figure 7 shows the comparison between the model predictions and numerical simulation results. The time evolution of the droplet shape [Fig. 7(a)] predicted by the model closely matches the numerical simulation [Fig. 7(b)], where the lamella elongates significantly along the direction of surface motion.

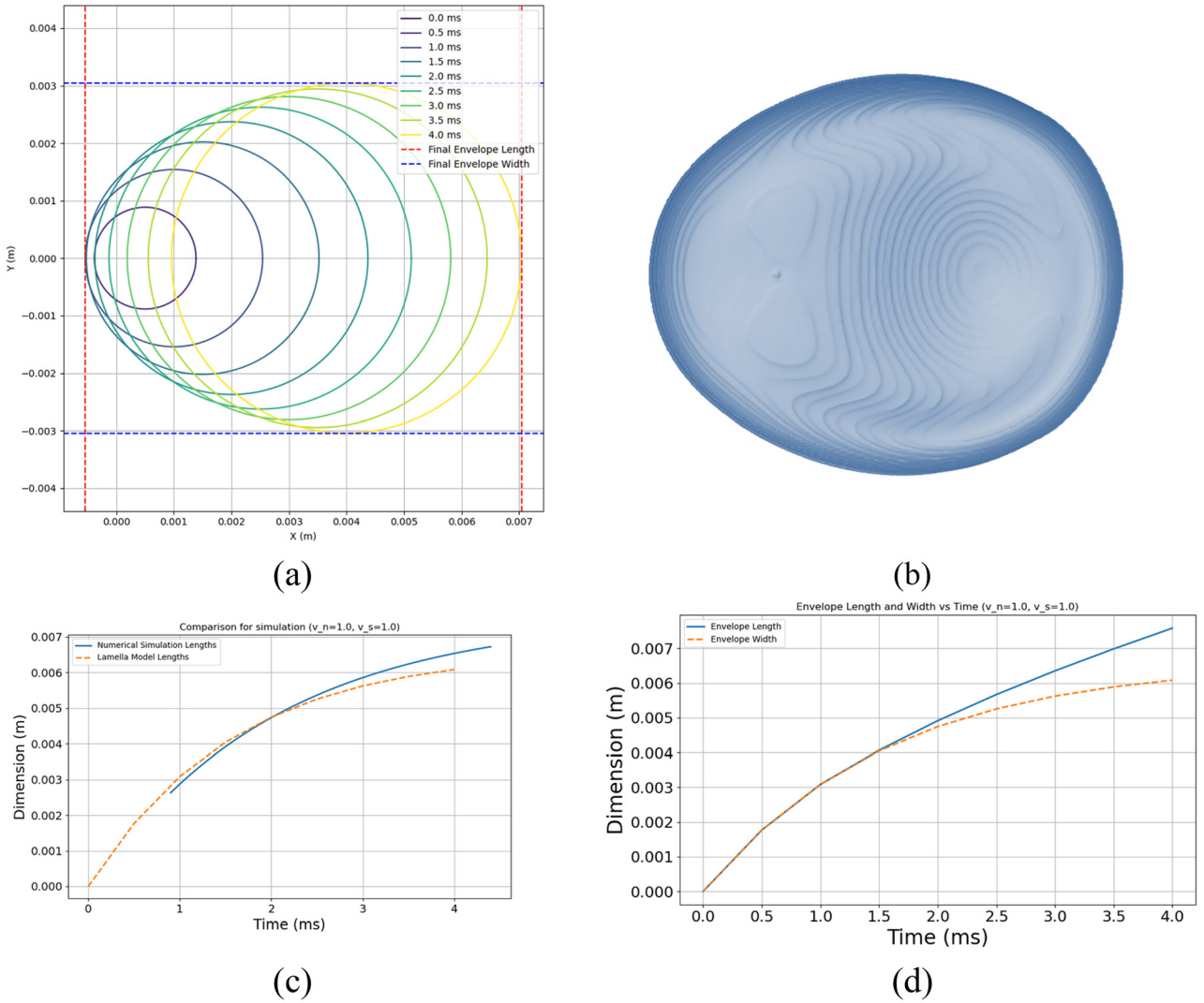

FIG. 7. Comparison of the modeled lamella shape with numerical simulation results for a moving surface. (a) Time evolution of the droplet shape from the model; (b) numerical simulation of the lamella at t = 4.0 ms; (c) comparison of the simulated and modeled lamella lengths; and (d) time evolution of the lamella length and width predicted by the model.

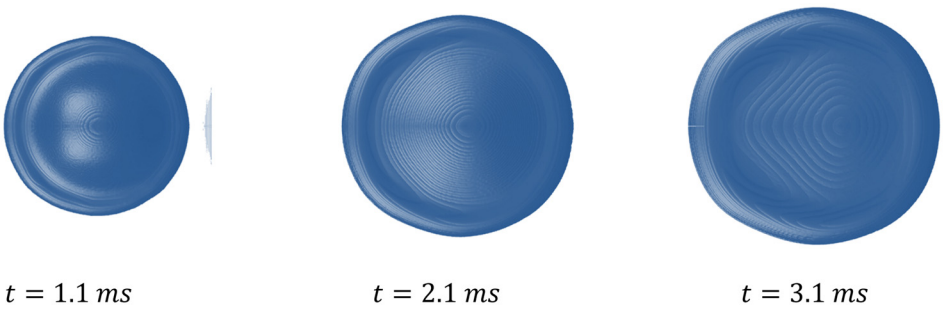

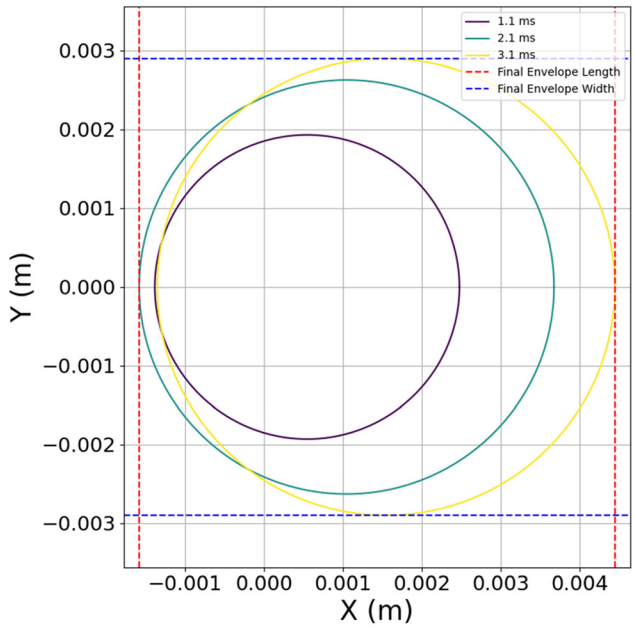

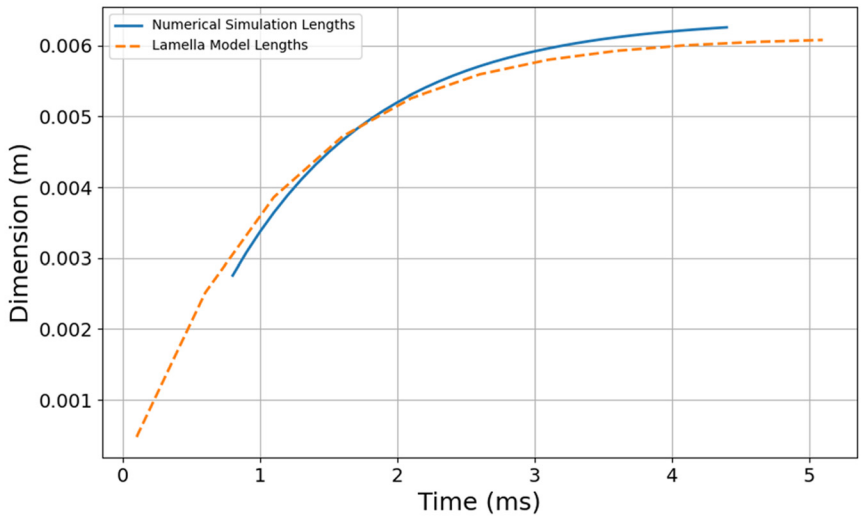

FIG. 8. Validation of the model's generalizability for $v_n = 1.2$ m/s and $v_s = 0.4$ m/s. The top row presents numerical simulation results (top view) at t = 1.1, 2.1, and 3.1 ms. The middle row shows the lamella shape evolution from the spreading model, and the bottom row compares the simulated and modeled lamella lengths over time.

A quantitative comparison of the lamella length [Fig. 7(c)] shows excellent agreement across all time intervals, with the model accurately capturing the nonlinear growth caused by the redistribution of kinetic energy along the motion axis. Additionally, the evolution of both the lamella length and width [Fig. 7(d)] confirms the development of asymmetry under surface motion, where the length continues to increase while the width stabilizes earlier. These results demonstrate the model's ability to incorporate surface velocity effects and predict the anisotropic spreading dynamics of non-Newtonian droplets. Now that the model has been validated for both static and moving surfaces, we examine its generalization capability under new velocity conditions.

3. Generalization and model robustness

The generalization capabilities of the refined model are evaluated under both trained and untrained conditions, as shown in Fig. 8. For trained conditions ($v_n = 1.5$ m/s and $v_s = 1.0$ m/s), the predicted lamella lengths closely match the numerical simulation results, validating the model's reliability. For untrained conditions ($v_n = 1.2$ m/s and $v_s = 0.4$ m/s), the model continues to perform accurately, capturing the lamella length and width evolution. The comparison of numerical and predicted lamella shapes at multiple time points highlights the model's ability to interpolate effectively within the parameter space defined by Weber and Ohnesorge numbers.

By aligning with scaling trends observed in Newtonian studies, the model demonstrates its robustness across diverse impact and surface velocities. Its capability to incorporate shear-thinning effects and predict delayed stabilization reinforces its suitability for practical applications, such as inkjet printing and coating processes.

IV. CONCLUSION

This study introduces a refined spreading model tailored to the unique dynamics of non-Newtonian droplets impacting stationary and moving surfaces. The model effectively integrates shear-thinning viscosity, inertial spreading, and capillary effects, extending the classical Newtonian frameworks. Validation against numerical simulations confirmed its ability to predict lamella dynamics, including anisotropic elongation, edge thinning, and delayed stabilization under varying impact and surface conditions.

For stationary surfaces, the model demonstrated accurate predictions of the lamella's time evolution, highlighting the significant role of shear-thinning effects in modulating spreading behavior. On moving surfaces, it successfully captured the transition from symmetric spreading to anisotropic deformation driven by surface motion, a key feature of non-Newtonian fluids. Moreover, the model exhibited robust generalization capabilities, maintaining high accuracy under untrained velocity conditions. Unlike previous models that primarily focus on Newtonian droplets or simplified spreading conditions, this refined approach successfully incorporates time-dependent shear-thinning viscosity effects, anisotropic spreading, and the influence of surface velocity. These advancements bridge critical gaps in existing predictive frameworks, offering a more comprehensive understanding of non-Newtonian droplet impact dynamics.

Despite its strong predictive capability, the model is currently limited to a specific range of shear-thinning fluids and assumes a constant ambient temperature. Future research should explore extending the model to viscoelastic fluids, incorporating temperature-dependent rheological effects, and validating results with high-speed experimental measurements. Additionally, further work could refine the model by integrating surface roughness effects and studying droplet impact on structured substrates, broadening its applicability to industrial and biomedical processes.

These findings provide a comprehensive understanding of non-Newtonian droplet dynamics, offering valuable insights for applications involving complex fluid interactions on dynamic surfaces. The refined model represents a significant advancement in predicting droplet spreading and can serve as a reliable tool for optimizing processes such as inkjet printing, spray coating, and pharmaceutical deposition. Future work may extend this framework to incorporate additional rheological complexities and explore its applicability to other fluid systems. By integrating additional rheological complexities in future iterations, this approach could further enhance predictive accuracy, ultimately improving process control in engineering and manufacturing applications.

ACKNOWLEDGMENTS

This work was supported by the PolyU Joint Postdoc Scheme (No. P0042938), the National Natural Science Foundation of China (Grant No. 52108268), the Key Laboratory of Hydraulic and Waterway Engineering of the Ministry of Education (No. SLK2023B18), the Fund of State Key Laboratory of Bridge Engineering Structural Dynamics, the Social Security Bureau, and the Chongqing Education Commission Youth Project.

AUTHOR DECLARATIONS

Conflict of Interest

The authors have no conflicts to disclose.

Author Contributions

Haicui Wang: Conceptualization (equal); Methodology (equal); Software (equal); Validation (equal); Visualization (equal); Writing – original draft (equal); Writing – review & editing (equal). **Long Shen:** Conceptualization (equal); Software (equal); Validation (equal); Visualization (equal); Writing – original draft (equal); Writing – review & editing (equal). **Lunliang Duan:** Conceptualization (equal); Investigation (equal); Methodology (equal); Resources (equal); Software (equal); Supervision (equal); Validation (equal); Visualization (equal); Writing – original draft (equal); Writing – review & editing (equal). **Xinxin Li:** Conceptualization (equal); Validation (equal); Visualization (equal); Writing – original draft (equal); Writing – review & editing (equal). **Zhimin Ma:** Conceptualization (equal); Validation (equal); Visualization (equal); Writing – original draft (equal); Writing – review & editing (equal). **Pengfei Li:** Conceptualization (equal); Visualization (equal); Writing – original draft (equal); Writing – review & editing (equal). **Kui Wang:** Conceptualization (equal); Writing – original draft (equal); Writing – review & editing (equal).

DATA AVAILABILITY

Data sharing is not applicable to this article as no new data were created or analyzed in this study.

REFERENCES

[1]C. Josserand and S. T. Thoroddsen, "Drop impact on a solid surface," Annu. Rev. Fluid Mech. **48**(1), 365–391 (2016).

[2]A. L. Yarin, "Drop impact dynamics: Splashing, spreading, receding, bouncing…," Annu. Rev. Fluid Mech. **38**(1), 159–192 (2006).
[3]B. Gorin, G. Di Mauro, D. Bonn, and H. Kellay, "Universal aspects of droplet spreading dynamics in Newtonian and non-Newtonian fluids," Langmuir **38**(8), 2608–2613 (2022).
[4]J. C. Bird, S. S. Tsai, and H. A. Stone, "Inclined to splash: Triggering and inhibiting a splash with tangential velocity," New J. Phys. **11**(6), 063017 (2009).
[5]N. Z. Mehdizadeh, M. Raessi, S. Chandra, and J. Mostaghimi, "Effect of substrate temperature on splashing of molten tin droplets," J. Heat Transfer **126**(3), 445–452 (2004).
[6]J. H. Snoeijer and B. Andreotti, "Moving contact lines: Scales, regimes, and dynamical transitions," Annu. Rev. Fluid Mech. **45**(1), 269–292 (2013).
[7]M. Abdelsayed, E. Trautner, J. Berchtenbreiter, and M. Klein, "Primary atomization of shear-thinning liquid jets: A direct numerical simulation study," Sci. Rep. **14**(1), 23896 (2024).
[8]L.-H. Luu and Y. Forterre, "Drop impact of yield-stress fluids," J. Fluid Mech. **632**, 301–327 (2009).
[9]P. Shah and M. M. Driscoll, "Drop impact dynamics of complex fluids: A review," Soft Matter **20**, 4839 (2024).
[10]R. Andrade, O. Skurtys, and F. Osorio, "Development of a new method to predict the maximum spread factor for shear thinning drops," J. Food Eng. **157**, 70–76 (2015).
[11]M. Guémas, Á. G. Marín, and D. Lohse, "Drop impact experiments of non-Newtonian liquids on micro-structured surfaces," Soft Matter **8**(41), 10725–10731 (2012).
[12]Y. Li, Z. Xu, X. Peng, T. Wang, and Z. Che, "Numerical simulation of secondary breakup of shear-thinning droplets," Phys. Fluids **35**(1), 012103 (2023).
[13]T. S. Mousavi, K. Sedighi, M. Farhadi, and E. Fattahi, "Lattice Boltzmann simulation of deformation and breakup of a droplet under gravity force using interparticle potential model," Int. J. Eng. **26**(7), 781 (2013).
[14]F. Boyer, E. Sandoval-Nava, J. H. Snoeijer, J. F. Dijksman, and D. Lohse, "Drop impact of shear thickening liquids," Phys. Rev. Fluids **1**(1), 013901 (2016).
[15]S. M. An and S. Y. Lee, "Maximum spreading of a shear-thinning liquid drop impacting on dry solid surfaces," Exp. Therm. Fluid Sci. **38**, 140–148 (2012).
[16]D. Yang, J. Chen, A. Shen, J. Wang, and H. Liu, "Spreading behaviors of shear-thinning droplets impacting on solid surfaces with various wettability," Korea-Aust. Rheol. J. **36**(3), 155–167 (2024).
[17]J. Cai, J. Ma, X. Chen, D. Liu, C. Liang, and S. Pan, "Numerical study on the dynamic behaviors of shear-thinning droplets impacting on a hydrophobic spherical surface," Phys. Fluids **36**(5), 053113 (2024).
[18]S. Chandra and C. Avedisian, "On the collision of a droplet with a solid surface," Proc. Roy. Soc. London. Ser. A: Math. Phys. Sci. **432**(1884), 13–41 (1991).
[19]M. H. Biroun *et al.*, "Impact dynamics of non-Newtonian droplets on superhydrophobic surfaces," Langmuir **39**(16), 5793–5802 (2023).
[20]S. M. Tilehboni, E. Fattahi, H. H. Afrouzi, and M. Farhadi, "Numerical simulation of droplet detachment from solid walls under gravity force using lattice Boltzmann method," J. Mol. Liq. **212**, 544–556 (2015).
[21]B. A. Nichita, I. Zun, and J. R. Thome, "A VOF method coupled with a dynamic contact angle model for simulation of two-phase flows with partial wetting," in 7th International Conference on Multiphase Flow, ICMF 2010, Tampa, FL, 30 May–4 June, 2010.
[22]J. U. Brackbill, D. B. Kothe, and C. Zemach, "A continuum method for modeling surface tension," J. Comput. Phys. **100**(2), 335–354 (1992).
[23]Y. D. Shikhmurzaev, "Moving contact lines and dynamic contact angles: A 'litmus test' for mathematical models, accomplishments and new challenges," Eur. Phys. J. Spec. Top. **229**(10), 1945–1977 (2020).
[24]R. Cox, "The dynamics of the spreading of liquids on a solid surface. Part 1. Viscous flow," J. Fluid Mech. **168**, 169–194 (1986).
[25]S. F. Kistler, "Hydrodynamics of wetting," Wettability **6**, 311–430 (1993).